RESEARCH ARTICLE

A Recurrent Activating Missense Mutation in Waldenström Macroglobulinemia Affects the DNA Binding of the ETS Transcription Factor SPI1 and Enhances Proliferation

Damien Roos-Weil[1,2,3,4,5], Camille Decaudin[1,2,3,4], Marine Armand[1,2,3,4], Véronique Della-Valle[1,2,3,4], M'boyba K. Diop[1,2,4,6], Hussein Ghamlouch[1,2,3,4], Virginie Ropars[7], Cécile Hérate[1,2,3,4], Diane Lara[1,2,3,4,8], Eric Durot[1,2,3,4], Rima Haddad[9], Elena Mylonas[1,2,3,4,10], Frederik Damm[10], Francoise Pflumio[9], Bilyana Stoilova[11], Marlen Metzner[11], Olivier Elemento[12], Philippe Dessen[1,2,3,4,6], Valérie Camara-Clayette[1,2,6], François-Loïc Cosset[13], Els Verhoeyen[13,14], Véronique Leblond[5], Vincent Ribrag[1,15], Pascale Cornillet-Lefebvre[16], Philippe Rameau[6], Nabih Azar[5], Frédéric Charlotte[5], Pierre Morel[17], Jean-Baptiste Charbonnier[7], Paresh Vyas[11], Thomas Mercher[1,2,3,4], Said Aoufouchi[2,3,4,18], Nathalie Droin[1,2,3,4,6], Christel Guillouf[1,2,3,4], Florence Nguyen-Khac[5,8], and Olivier A. Bernard[1,2,3,4]

ABSTRACT

The ETS-domain transcription factors divide into subfamilies based on protein similarities, DNA-binding sequences, and interaction with cofactors. They are regulated by extracellular clues and contribute to cellular processes, including proliferation and transformation. *ETS* genes are targeted through genomic rearrangements in oncogenesis. The *PU.1/SPI1* gene is inactivated by point mutations in human myeloid malignancies. We identified a recurrent somatic mutation (Q226E) in *PU.1/SPI1* in Waldenström macroglobulinemia, a B-cell lymphoproliferative disorder. It affects the DNA-binding affinity of the protein and allows the mutant protein to more frequently bind and activate promoter regions with respect to wild-type protein. Mutant SPI1 binding at promoters activates gene sets typically promoted by other ETS factors, resulting in enhanced proliferation and decreased terminal B-cell differentiation in model cell lines and primary samples. In summary, we describe oncogenic subversion of transcription factor function through subtle alteration of DNA binding leading to cellular proliferation and differentiation arrest.

SIGNIFICANCE: The demonstration that a somatic point mutation tips the balance of genome-binding pattern provides a mechanistic paradigm for how missense mutations in transcription factor genes may be oncogenic in human tumors.

[1]INSERM U1170, Gustave Roussy, Villejuif, France. [2]Gustave Roussy, Villejuif, France. [3]Université Paris-Saclay, Villejuif, France. [4]Equipe labellisée Ligue Nationale Contre le Cancer, Paris, France. [5]Sorbonne Université, Hôpital Pitié-Salpêtrière, APHP, Paris, France. [6]AMMICa, INSERM US23/CNRS UMS3655, Gustave Roussy, Villejuif, France. [7]Institute for Integrative Biology of the Cell (I2BC), Institute Joliot, CEA, CNRS, Univ. Paris-Sud, Université Paris-Saclay, Gif-sur-Yvette cedex, France. [8]Sorbonne Université, INSERM UMRS 1138, Centre de Recherche des Cordeliers, Paris, France. [9]Commissariat à l'Energie Atomique et aux Energies Alternatives (CEA) DSV-IRCM-SCSR-LSHL, Université Paris Diderot Sorbonne Paris Cité, Fontenay-aux-Roses, France. [10]Department of Hematology, Oncology and Tumor Immunology, Charité-Universitätsmedizin Berlin, Corporate Member of Freie Universität Berlin, Humboldt-Universität zu Berlin, and Berlin Institute of Health, Berlin, Germany. [11]MRC Molecular Haematology Unit, MRC Weatherall Institute of Molecular Medicine, NIHR Oxford Biomedical Research Centre Haematology Theme, Radcliffe Department of Medicine and Department of Haematology, Oxford University and Oxford University Hospitals NHS Foundation Trust, United Kingdom. [12]Department of Physiology and Biophysics, Institute for Computational Biomedicine, Caryl and Israel Englander Institute for Precision Medicine, Weill Cornell Medicine, New York, New York. [13]CIRI–International Center for Infectiology Research, Team EVIR, Université de Lyon; INSERM, U1111; Ecole Normale Supérieure de Lyon; Université Lyon 1; CNRS, UMR5308, Lyon, France. [14]Université Côte d'Azur, INSERM, C3M, Nice, France. [15]DITEP Gustave Roussy, Villejuif, Paris, France. [16]Laboratoire d'hématologie, Pôle de biologie, CHU de Reims-Hôpital Robert Debré, Avenue du Général Koenig, Reims, France. [17]Centre Hospitalier Dr. Schaffner, Lens; Service d'Hématologie Clinique et Thérapie Cellulaire, CHU Amiens Picardie, Amiens cedex, France. [18]CNRS UMR8200, Gustave Roussy, Villejuif, France.

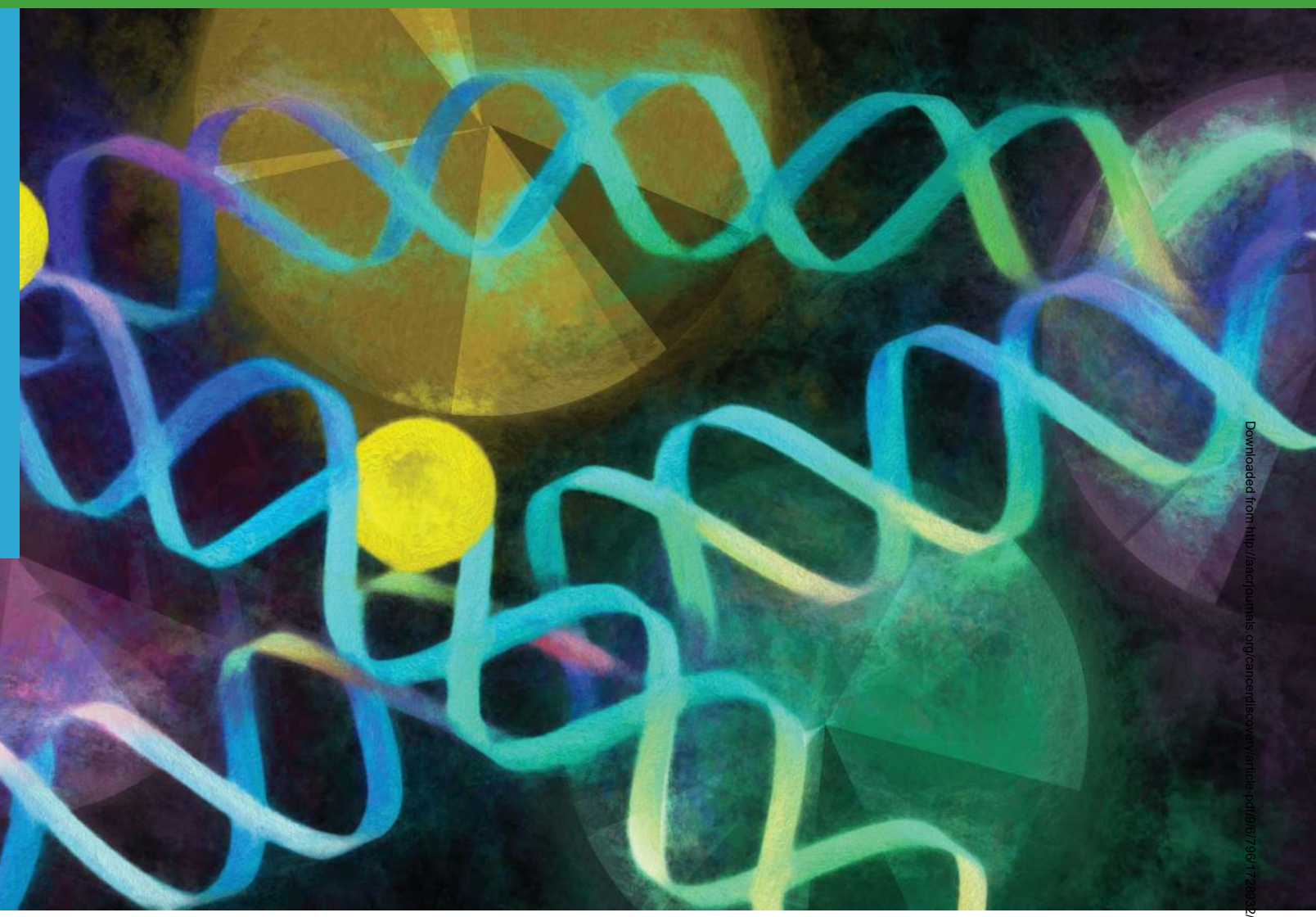

INTRODUCTION

B-cell differentiation is a multistep process that starts in the bone marrow and continues in periphery. B cells activated by antigen contact undergo affinity maturation in the germinal center (GC) allowing generation of mature plasma cells excreting high-affinity immunoglobulins and memory B cells, keeping the souvenir of antigen encounter (1). B-cell differentiation and maturation are tightly controlled by precise tuning of epigenetic, intracellular signaling pathways [especially B-cell receptor (BCR) and Toll-like receptor (TLR)], and activity of transcription factors, including the ETS family (1, 2). The ETS family of transcription factors shares a conserved winged helix-turn-helix DNA-binding domain (DBD) and binds to a consensus DNA sequence containing a core 5′-GGA(A/T)-3′ motif (3). ETS factors regulate gene expression through binding to ETS motifs or to composite sites through interaction with other transcription factors, including IRF4, IRF8, CÆBPα and CÆBPβ, and c-Jun (4). SPI1 is an ETS family member that plays a crucial role in hematopoiesis (5–7), including at different steps of B-cell development, coordinating the proliferation and differentiation of B-lymphoid progenitors, but also acting as a repressor of terminal B-cell differentiation (8, 9). In humans, inactivating *SPI1* mutations

Note: Supplementary data for this article are available at Cancer Discovery Online (http://cancerdiscovery.aacrjournals.org/).

D. Roos-Weil, C. Decaudin, and M. Armand contributed equally to this article.

F. Nguyen-Khac and O.A Bernard are co–senior authors of this article.

Corresponding Authors: Olivier A. Bernard, INSERM U1170, Gustave Roussy, 39 rue Camille Desmoulins, Villejuif Cedex 94805, France. Phone: 331-4211-4233; Fax: 331-4211-5101; E-mail: olivier.bernard@inserm.fr; and Florence Nguyen-Khac, Unité de Cytogénétique Hématologique, Service d'Hématologie Biologique, GH Pitié-Salpêtrière/Charles Foix, 83 Bd de l'Hôpital, Paris 75013, France. E-mail: florence.nguyen-khac@aphp.fr

Cancer Discov 2019;9:796–811

doi: 10.1158/2159-8290.CD-18-0873

have been described in acute myeloid leukemia (AML; refs. 10, 11) and gene fusions involving *SPI1* have been identified in pediatric T-cell acute lymphoblastic leukemia (12).

Biological processes driving GC reaction or generation of antibody-secreting plasma cells can be somatically altered leading to B-cell lymphoma and multiple myeloma (1). Activating mutations targeting genes encoding proteins that convey proliferative signals downstream of antigen exposure and BCR signaling include the adapter protein MYD88 (13). Activating mutations of *MYD88* [the most frequent is L265P (LP)] are observed in a wide range of mature B-cell tumors and lead to constitutive activation of the NF-κB and JAK signaling pathways (13).

Waldenström macroglobulinemia (WM) is defined as an IgM-secreting and bone marrow–infiltrating lymphoplasmacytic lymphoma, related to memory B cells and shows a *MYD88* mutation in more than 95% of cases (14). Despite its indolent nature and treatment advances, WM remains incurable, with most patients dying from disease progression, underscoring the need of more specific targeted therapies. This relies on better understanding of the genetic landscape and mechanisms of transformation. Here, we describe the somatic mutational landscape of WM and identify a novel recurrent activating somatic mutation of the hematopoietic transcription factor *SPI1*. The mutation subtly alters DNA-binding sequence preference, changing the patterns of genes activated from ones normally activated by SPI1 to those more typically activated by other ETS family members. Cumulatively, the altered gene expression programs result in oncogenic proliferative signaling and a block in B-cell differentiation.

RESULTS

Identification of a Recurrent *SPI1* Mutation in WM

To gain insights into WM physiopathology, we compared tumor and CD3$^+$ germline coding sequences of a discovery cohort of 16 patients with WM and identified 265 somatic mutations affecting 230 genes, corresponding to a median of 16.5 mutations per patient (Methods; Supplementary Tables S1–S3; Supplementary Fig. S1A–S1C). In addition, we analyzed an extended cohort of 69 patients with WM, by targeted sequencing of 20 recurrently mutated genes (Supplementary Tables S4 and S5, for coordinates and mutations, and Supplementary Fig. S1D and S1E for summary). The distribution and frequency of mutations in the 85 patients with WM is shown in Fig. 1A. *MYD88* (81/85, 95%), *CXCR4* (24/85, 28%), and *ARID1A* (7/85, 8%) were confirmed to be the most frequently mutated genes in WM. Among the 13 genes mutated in at least 2 patients, 12 (*MYD88, IGLL5, CXCR4, ARID1A, CD79B, TP53, LTB, HIST1H1E, TRAF2, ROBO2, TRRAP, EZH2*) had been previously identified in the context of WM or other B-lymphoid malignancies (14, 15).

A novel mutation in the transcription factor gene *SPI1* was observed in 5 of 85 patients with WM (5.9%) of both discovery (2/16) and validation (3/69) cohorts (Fig. 1A). All patients carried the same single-nucleotide change (C>G) leading to a Gln (Q) for Glu (E) amino acid change at position 226 (Q226E, QE) in the ETS domain of the protein (Fig. 1B). This mutation was not detected in the matched T-cell fraction. The Q226 residue lies within the alpha 3 helix of the DBD and is a conserved amino acid specific for the class III subgroup of the ETS proteins, substituted by E in classes I and IIa proteins (Fig. 1C). The mutations were observed on both DNA and RNA sequences from flow-sorted tumor cells (Fig. 1D, left and middle), at clonal or subclonal levels (Fig. 1B). *SPI1* transcription was similar between *SPI1* wild-type (WT) and QE samples (Fig. 1D, right). This mutation was not reported in the Catalogue of Somatic Mutations in Cancer (COSMIC; v87) database and not observed in a large number of other B-cell lymphoproliferative disorders samples (Supplementary Fig. S1F), indicating it might be specific to WM. Its stereotyped and heterozygous nature suggests it represents an example of *SPI1*-activating mutations in humans.

Biological and Clinical Features of *SPI1*-Mutated Patients

The main clinical and biological characteristics of the patients with WM are presented in Supplementary Table S1. Most characteristics were similar between the *SPI1* WT and QE subgroups with the exception of a significantly higher proportion of pejorative WM International Prognostic Scoring System prognostic features (16) in the *SPI1*-mutated subgroup. Analyses of bone marrow biopsy samples for CD38 and CD138 B-cell differentiation markers showed fewer CD138$^+$ cells in mutant *SPI1* samples, suggesting less differentiation, with respect to *SPI1* WT patients (Fig. 1E; Supplementary Fig. S2A and S2B).

When compared with *SPI1* WT cases, mutant *SPI1* cases exhibited significantly shorter overall survival (OS), with median survival times that were, respectively, not reached and 20.7 months [HR = 7.39; 95% confidence interval (95% CI), 1.5–89; log-rank $P = 0.0004$; Fig. 1F]. Although it was not significant, *SPI1*-mutated patients showed a trend to shorter time to relapse and to next treatment compared with *SPI1* WT cases (log-rank $P = 0.13$ and 0.36). OS of *SPI1*-mutated patients was also shorter than that of *CXCR4*-mutated patients, a previously described aggressive subgroup of patients with WM (Supplementary Fig. S2C–S2K; log-rank $P = 0.0003$).

Mutant SPI1 Maintains DNA-Binding and Transactivation Capacities and Increases Cellular Proliferation

SPI1 Q226 lies at a position that specifies the -2 position upstream of the GGAA ETS-core sequence, which represents one of the differences between SPI1 and other ETS-binding sites (17). We first used electrophoretic mobility shift assays (EMSA) to confirm the binding of SPI1 QE protein to the ETS-DNA motif derived from a known SPI1 target (18). A specific shifted complex was observed with the *Fes* probe (Fig. 2A; Supplementary Fig. S3A). Using isothermal calorimetry, we then compared binding affinity of GST fusion proteins containing the WT or mutant DNA-binding domains of SPI1 to lambda B1, a classic SPI1-binding site (19), and mutants thereof. A higher affinity to the WT lambda B1 sequence was observed for the SPI1 WT protein compared with QE protein (the affinity constant of the WT protein was 2.7 times lower). The opposite was observed for the SPI1 consensus sequence mutated into an ETS1-like sequence by

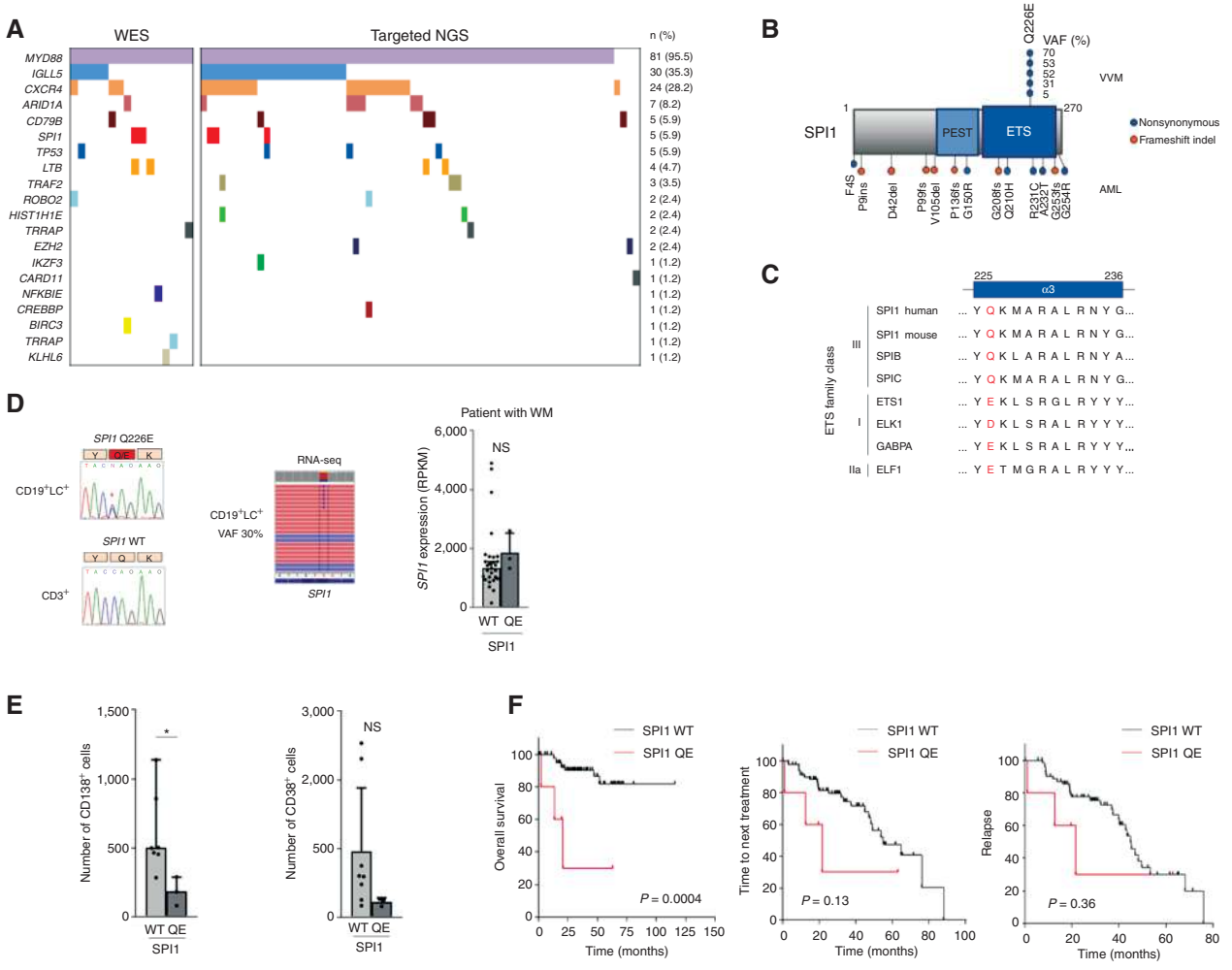

Figure 1. Mutational analyses of WM identify an acquired recurrent *SPI1* missense mutation. **A,** Mutational landscape of 85 patients with WM analyzed by WES ($n = 16$) and targeted ($n = 69$) sequencing. Each column represents a patient sample and each row a mutated gene. The number and percentage of each mutated gene in the whole cohort are indicated on the right of the grid. NGS, next-generation sequencing. **B,** Locations of *SPI1* mutations identified in WM ($n = 85$) and AML ($n = 541$) samples (10, 11). *SPI1* mutations are indicated at their amino acid position, color-coded by type of mutation (orange, frameshift; blue, nonsynonymous). Inactivating mutations observed in AML are shown beneath the protein, whereas WM QE mutations appear above. The estimated VAF in the 5 patients with WM and identified functional domains are indicated. PEST, proline-, glutamic acid–, serine-, and threonine-rich domain; ETS, ETS DNA-binding domain. Q, glutamine; E, glutamic acid; VAF, variant allele frequencies. **C,** Sequence alignment of members of ETS family proteins, in the vicinity of glutamine (Q) amino acid (red) lying at position 226 in alpha helix H3 of the conserved ETS domain. Numbers above indicate positions of amino acids of the human protein. **D,** Left, illustration of the *SPI1* Q226E (QE; c.676C>G, p.Gln226Glu) missense mutation detected in DNA from flow-sorted CD19 and light chain (LC)–positive tumor cells (top, left), as compared with matched $CD3^+$ T cells of the same patient (bottom, left). A red star indicates the mutant base. Middle, expression of the mutant copy in RNA-seq data from the same patient is shown. Right, normalized read counts mapping to *SPI1* exons 1–5 are plotted to compare expression levels of *SPI1* transcripts in *SPI1* WT ($n = 29$) and QE ($n = 3$) WM samples. Histograms, median and bars 95% CI. Statistics were performed using Student *t* test. NS, not significant. **E–F,** Biological and clinical features of *SPI1* Q226E mutations in WM. **E,** Expression of differentiation markers analyzed by IHC on bone marrow biopsy samples of *SPI1* WT ($n = 8$) and QE ($n = 3$) patients with WM. The numbers of $CD38^+$ and $CD138^+$ plasma cells were evaluated on randomly placed squares representing a median whole area of 0.9 mm^2. Error bars, SD. Statistics were performed using Student *t* test. NS, not significant. *, $P \leq 0.05$. **F,** Kaplan–Meier survival curves of overall survival (left), time to next treatment (middle) and relapse-free survival (right) for patients with ($n = 5$) and without ($n = 80$) *SPI1* QE mutation. *P* values are indicated and based on the log-rank test.

a double CC to AA mutation (at position -2 and -1 upstream of the GGAA core sequence). None of the proteins showed significant binding toward a mutant ETS core site (Fig. 2B; Supplementary Fig. S3B–S3F).

To evaluate the transcriptional potential of the mutant protein, we performed luciferase assays with reporter constructs containing the *Fes* promoter region (Fig. 2C), the lambda B1 site (Fig. 2D), or the ETS1-binding sequence of the human *GPAA1* gene promoter (Fig. 2E), a gene bound by SPI1 QE in OCI-Ly10 cells (Supplementary Fig. S4A). Dose-dependent transcriptional activity was observed for both WT and QE proteins on each of the studied constructs that was abolished when the ETS-core sequence was mutated (Fig. 2C–E; Supplementary Fig. S3G–S3H). We noticed differences in the transcriptional activation capacities of the two proteins depending on the tested target. Up to two-fold more activation

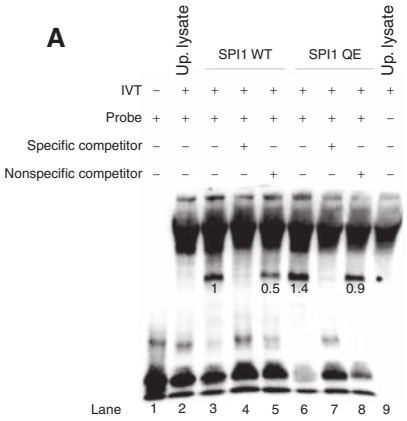

B

Motif type	Sequence	Protein	K_d (nmol/L)
SPI1	AAGGAAGTG	GST-SPI1(WT)	0.42 ± 0.08
		GST-SPI1(QE)	1.14 ± 0.08
		GST	NI
ETS1-like	CCGGAAGTG	GST-SPI1(WT)	7.2 ± 1.8
		GST-SPI1(QE)	2.5 ± 0.7
Mutant	AACCAAGTG	GST-SPI1(WT)	NI
		GST-SPI1(QE)	NI

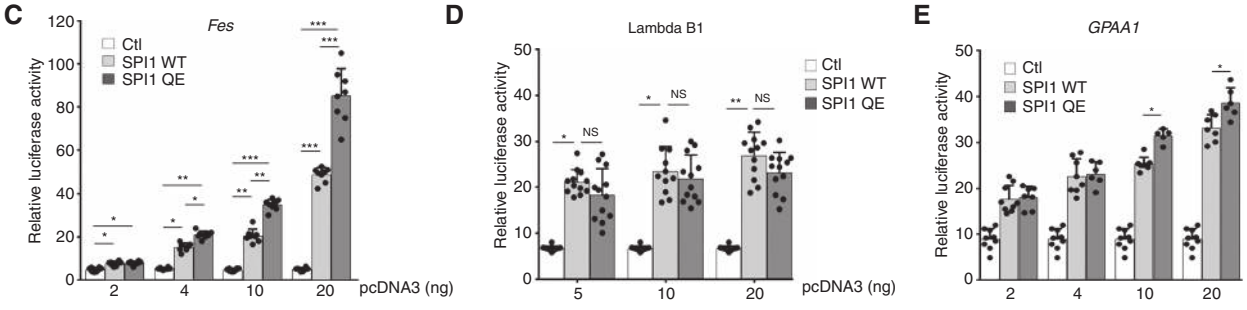

Figure 2. DNA-binding and transcriptional activation properties of mutant SPI1. **A,** Mutant SPI1 binds to ETS motif sequences. EMSA of control (up. lysate, unprogrammed lysate), SPI1 WT and QE IVT proteins in the presence of an ETS motif–containing probe with (+) or without (–) a 160× excess of a specific or nonspecific competitor, as indicated. The ETS motif–containing probe and competitors are from ref. 18. Sequences are provided in Methods. Estimation of the DNA-binding complex intensity in the different conditions is represented. Protein quantities produced by the indicated IVT lysates were similar (Supplementary Fig. S3A). IVT, *in vitro* translation; up., unprogrammed. **B,** *In vitro* comparison of DNA-binding affinities shows differences between SPI1 WT and QE proteins. Affinity was measured by isothermal calorimetry of the DNA-binding domain of SPI1 in fusion with GST with different DNA sequences. GST alone shows no high affinity site. The control DNA, with a GGAA > CCAA mutation in the core ETS-binding motif, demonstrated no high-affinity site. NI, no interaction. **C–E,** Mutant SPI1 transactivates a variety of ETS-reporter constructs. HEK293T cells were transfected with increasing amounts of the indicated [control (Ctl), SPI1 WT, or QE] expression plasmids and fixed amounts of a luciferase reporter gene. Reporter genes contain three copies of the following ETS motifs: *Fes* (**C**), lambda B1 (**D;** see **B** for motif), and *GPAA1* promoter (CCGGAAGTG; **E**). Sequences are provided in Methods. Three independent experiments were performed ($n = 8$–9; mean ± SD). Error bars, SD. *, $P \le 0.05$; **, $P \le 0.01$; ***, $P \le 0.001$.

was observed for SPI1 QE on the *Fes* promoter, whereas the two proteins showed similar activity on the SPI1-specific lambda B1 site. A stronger activation was observed with SPI1 QE at the highest doses on the ETS site of the *GPAA1* promoter. These *in vitro* experiments show that while maintaining the binding and transactivation capacity of the protein, the mutation differentially affects SPI1 activity depending on the tested region. More precisely, it appears that SPI1 QE retains binding and transactivation capacity on the classic SPI1-binding site but has an increased affinity and transactivation capacity on ETS1-like binding sites.

To gain insight into SPI1 QE binding to DNA on a genome-wide scale, we performed a chromatin immunoprecipitation sequencing (ChIP-seq) experiment with OCI-Ly10 cells expressing GFP fused to SPI1 WT or QE in an inducible fashion (Supplementary Fig. S4B and S4C). ChIP-seq performed with anti-GFP or anti-SPI1 antibodies showed similar results [Fig. 3A and B; Supplementary Tables S6–S9 (for anti-GFP); Supplementary Fig. S4D and S4E and Supplementary Tables S10–S13 (for anti-SPI1)].

DNA motif analyses of SPI1 WT- and QE-specific peaks identified different preferential motifs. The classic SPI1 motif was at the top of the motif list bound by SPI1 WT (Fig. 3A), whereas it ranked in 10th position for SPI1 QE (Fig. 3B). The top hit of motifs recognized by SPI1 QE is a common class I/IIa (ETS1/GABPA/ELF1/ELK1) motif (Fig. 3B). These two motifs differ in a single nucleotide (G or C) at position -2 of the core GGA(A/T), as clearly shown by the *de novo* analysis (Fig. 3C). Classes I/IIa motifs were observed in 77 and 95% (χ^2 $P = 2.2 \times 10^{-90}$) and class III motifs in 85 and 57% (χ^2 $P = 8.0 \times 10^{-163}$) of SPI1 WT and QE peaks, respectively (Supplementary Tables S6–S9). The composite SPI-IRF site dropped from 9th in SPI1 WT to 19th rank in SPI1 QE. These data are in line with DNA-binding affinity, as evaluated by isothermal calorimetry (Fig. 2B) and the *in vitro* analyses of ETS family DNA-binding properties, which pointed at Q226 of SPI1 (class III) and E226 of ELF1 (class IIa) for recognizing G or C at position -2 (17). In addition, gene set enrichment analyses (GSEA) using gene sets specific for ETS1, ELK1, and GABPA indicate that SPI1 QE transcriptional activation in

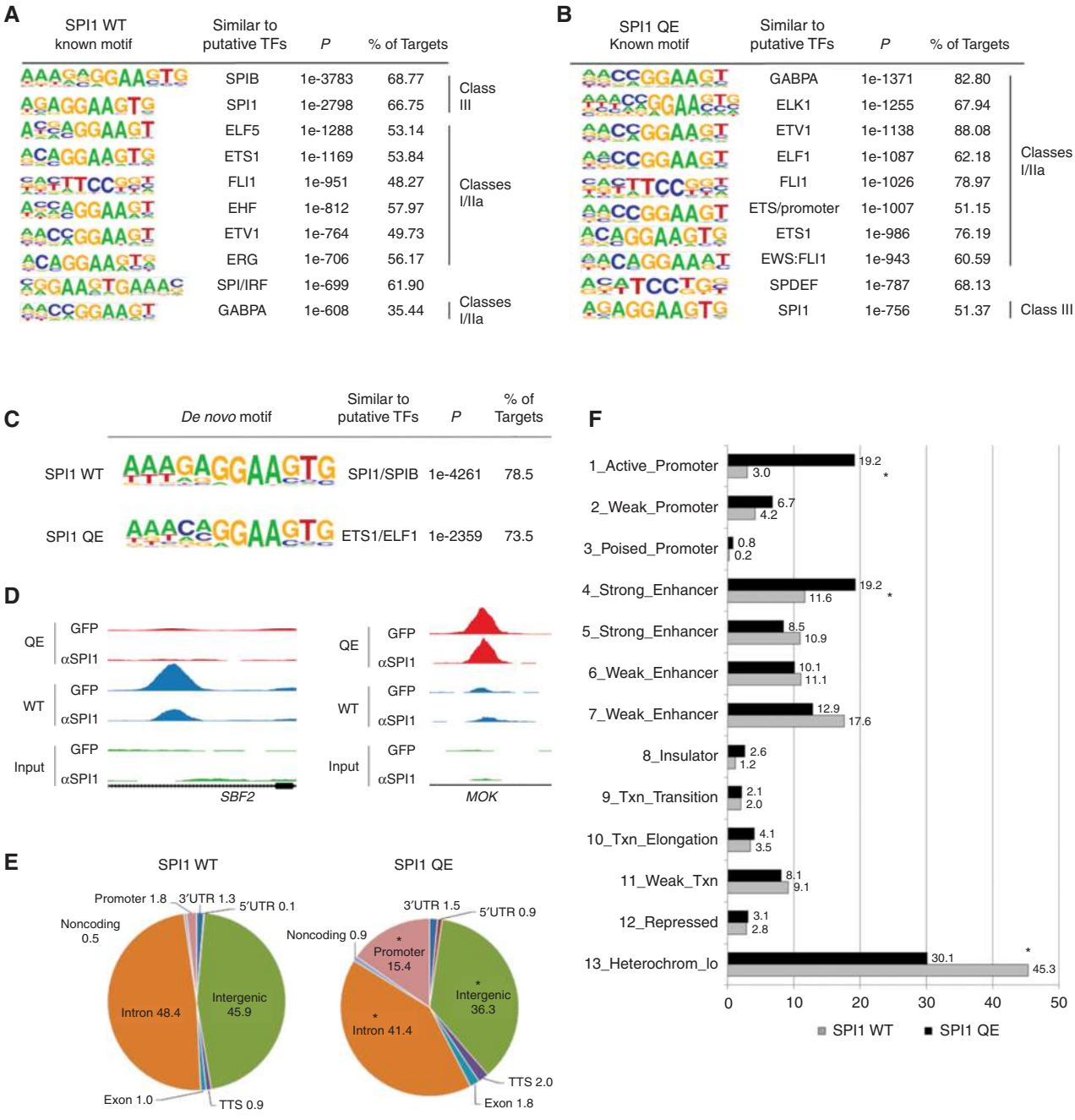

Figure 3. DNA-binding profile of mutant SPI1 in human B-cell lymphoma cell line. **A–F,** ChIP-seq analyses, performed with anti-GFP-Trap antibodies, in OCI-Ly10 cells transduced with doxycycline-inducible vectors expressing SPI1 WT or QE. Commonest known (**A** and **B**) and *de novo* (**C**) DNA motifs recognized by SPI1 WT (**A**) and QE (**B**) proteins. Homer motif known and *de novo* analyses were performed with a cut-off *P* value of 10^{-30}. The complete lists of *de novo* and known motifs are available in Supplementary Tables S6–S9 and S10–S13 for ChIP experiments performed with anti-GFP and anti-SPI1 antibodies, respectively. Motifs, associated transcription factors, *P* values, and percentages of peaks containing the motifs are indicated. **D,** ChIP-seq normalized signals with SPI1 QE (red) and WT (blue) proteins along with the input (green) are shown for two examples of differentially bound genes. The results of ChIP-seq data performed with GFP-Trap (top, GFP) and anti-SPI1 (bottom, αSPI1) antibodies are shown. *SBF2*: FDR = 0.00162; *MOK*: FDR = 0.00562. Genomic localization, defined by RefSeq (**E**) or ChromHMM (**F**; ref. 20) annotations, of DNA sequences (peaks) bound by SPI1 WT (left or gray) and QE (right or black; GFP) proteins. Different genomic regions and their respective percentage (with respect to the total number of peaks) are indicated. Statistics comparing the repartition of genomic regions were performed using χ^2 test. *, $P \leq 0.05$. TF, transcription factors; TTS, transcription termination sites; UTR, untranslated regions.

OCI-Ly10 cells more closely resembles ELK1 and ETS1-associated gene profiles (see Fig. 6B).

Examples of SPI1 QE- and WT-specific peaks are shown in Fig. 3D. Genomic regions bound by SPI1 QE were significantly enriched in promoters (defined by RefSeq; Fig. 3E), and in active promoters and strong enhancers (defined by ChromHMM annotations; Fig. 3F; ref. 20). Our data are consistent with frequent binding of classes I/IIa proteins at promoters, in contrast with what is observed for SPI1, in an Epstein-Barr virus–transformed B-cell line (Supplementary Fig. S4F and S4G and Supplementary Table S14).

Collectively, these data show that the *SPI1* QE mutation modifies the genome-wide DNA-binding pattern of the protein in a subtle way, in terms of both motif and localization, resulting in a specific transcriptional response.

We next investigated the effect of mutant SPI1 on cellular parameters. We first tested OCI-Ly10 cells that were stably transduced with doxycycline-inducible constructs encoding GFP [control (Ctl)] or GFP–SPI1 fusion proteins (WT or QE) and incubated or not with doxycycline for 48 hours. Both proteins were expressed at similar levels (Supplementary Fig. S4B). Both SPI1 WT and QE-expressing cells expanded in numbers significantly more than cells harboring the control construct (SPI1 WT cells expanded cell numbers twice as much and there were 20% more cells containing the SPI1 QE construct than the WT; Fig. 4A). To confirm this observation in another cellular context, we similarly overexpressed WT and mutant SPI1 proteins in BCWM.1 and MWCL-1 cell lines, established from *MYD88* LP WM samples. In both cell lines, overexpression of SPI1 QE resulted in more proliferation than overexpression of the WT form (see Fig. 6F and H). However, the OCI-Ly10 cell line represents a cleaner model than BCWM.1 and MWCL-1 cells for the functional investigations of SPI1 proteins, given the lack of detectable endogenous SPI1 expression in OCI-Ly10, unlike BCWM.1 and MWCL-1 (Supplementary Fig. S4B and S5A–S5D). Cell-cycle analyses in OCI-Ly10 cells showed that ectopic SPI1 expression decreased the percentage of cells in G_1 phase and proportionately increased cells in G_2–M phase (Fig. 4B–E). Similar variations of higher amplitude were observed in cells expressing SPI1 QE. These data indicate that mutant SPI1 likely promotes expansion via cellular proliferation in a manner that is similar to, but greater than SPI1 WT.

To characterize the consequences of mutant SPI1 binding, we used RNA sequencing (RNA-seq) to compare OCI-Ly10 cells expressing SPI1 WT or QE proteins. By GSEA, we observed that, as compared with SPI1 WT, expression profiles of mutant SPI1 samples were significantly enriched for functional annotations related to proliferation, cell cycle but also signal transduction programs that are central to B-cell physiology and pathology, including MYC, BCR, CD40 receptor (CD40), TLR, and PI3K signaling pathways (Fig. 4F; see Supplementary Table S15 for the list of enriched signatures). Differential expression was observed for target genes of key B-cell transcription factors, including XBP1, PRDM1, and IRF4 when signatures from the Lymphochip database (21) were used (Fig. 4F). These data confirm that SPI1 QE affects cellular proliferation to a higher extent than SPI1 WT.

SPI1 Mutation Cooperates with *MYD88*L265P and Interferes with Terminal B-cell Maturation in Murine Primary B Cells

We next investigated the effects of mutant SPI1 on hematopoietic and B-cell development in primary cells. To determine the effect of mutant SPI1 on hematopoietic development, mouse progenitor cells were transduced to express either SPI1 WT or QE and transplanted into lethally irradiated mice. SPI1 expression promoted accumulation of GFP^+ cells in bone marrow and myeloid differentiation at the expense of B-lymphoid differentiation (Supplementary Fig. S6A–S6C). Mature B cells were significantly fewer and differentiation of B-lymphoid progenitors was abnormal with more cells accumulating at an earlier stage in SPI1 QE condition compared with SPI1 WT (Hardy's fraction A vs. B and C; Supplementary Fig. S6D). These data are consistent with previous reports describing SPI1 as a determinant of lymphoid and myeloid fate choices; high SPI1 levels favor the development of myeloid cells whereas B-cell development requires its downregulation (22) and indicates that SPI1 QE behaves as SPI1 WT in those settings. No transformation was observed during an 18-month follow-up.

Because *SPI1* QE mutations are detected in association with *MYD88* LP, we constructed retroviral vectors driving expression of MYD88 and SPI1 (WT or mutant) either alone or in combination (Fig. 5A) to investigate potential oncogenic cooperation. All constructs expressed comparable levels of proteins (Supplementary Fig. S7A and S7B). Naïve B-lymphocytes were purified from WT mice, stimulated, and transduced by retroviral constructs (Fig. 5B), and the proportion of fluorescent cells was monitored in the culture, as described previously (23). Ectopic expression of MYD88 WT, SPI1 WT, or the empty backbone vector did not confer growth capacities to the transduced cells, whereas expression of mutant SPI1 expanded cell survival (Fig. 5C). As already reported (23), expression of mutant MYD88 conferred a growth advantage over B cells expressing WT constructs. This advantage was statistically increased when SPI1 QE, but not WT, was coexpressed with MYD88 LP, indicating cooperation between those two mutants. We also investigated the consequences on lymphocyte maturation toward plasmablastic/plasmacytic cells by examining the proportion of GFP^+ B cells (CD19) expressing CD138, a marker of terminal B-cell differentiation. Expression of MYD88 did not markedly affect the proportion of $CD138^+$ B cells, whereas expression of SPI1, WT or QE, alone or in combination with MYD88 LP, decreased the proportion of this cell population (Fig. 5D and E). The drop in the ratio of $CD138^+$ B cells was more important when SPI1 was expressed alone. In contrast to cellular growth, SPI1 WT or QE did not differentially affect the differentiation ratio in these conditions.

To extend our investigation, we compared RNA-seq data from MYD88 LP, MYD88 LP-SPI1 WT (LP/WT), and MYD88 LP-SPI1 QE (LP/QE)–expressing cells. In keeping with increased proliferation, MYC, E2F, and JAK–STAT signatures were enriched in SPI1 QE–expressing cells, with respect to SPI1 WT (Supplementary Fig. S7D–S7F).

To confirm our observations that SPI1 QE interferes with B-cell differentiation and their relevance in primary

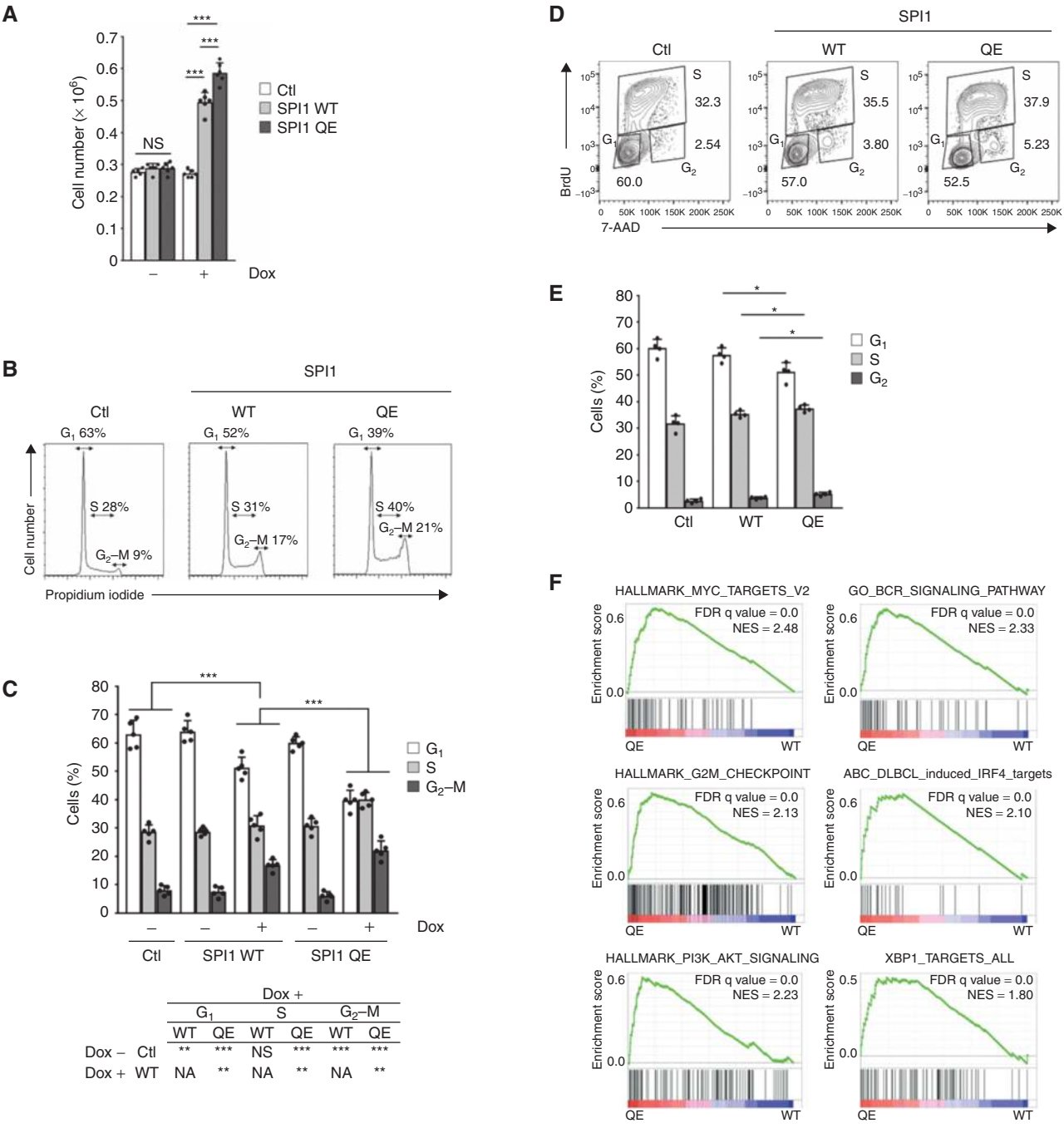

Figure 4. Cellular effects of mutant SPI1. **A,** Induction of SPI1 stimulates cellular proliferation. Quantitation of *in vitro* proliferation for OCI-Ly10 cells transduced with doxycycline-inducible constructs encoding GFP (Ctl), or SPI1-GFP fusion proteins (either WT or QE; $n = 6$, mean ± SD), with (+) or without (–) the 48-hour addition of doxycycline. The levels of SPI1 proteins and their nuclear localization were checked in OCI-Ly10 cells bearing the different constructs (Supplementary Fig. S4B and S4C), and found to be equivalent for SPI1 WT and QE conditions. NS, not significant. ***, $P \leq 0.001$. Statistics were performed using two-tailed Student *t* test. Error bars, SD. **B–E,** Cell-cycle analyses in OCI-Ly10 cells transduced with doxycycline-inducible constructs encoding GFP (Ctl), or SPI1-GFP fusion proteins (either WT or QE). Representative flow cytometry analyses (**B**) of propidium iodide DNA staining of OCI-Ly10 cells bearing the indicated constructs and estimation (in %; **C**) of the fraction of cells in G_1–S–G_2–M cell-cycle phases. Cell cultures were treated with ($n = 5$) or without ($n = 5$) doxycycline during 24 hours before staining. The table beneath the graph details statistical comparisons between different conditions. Representative flow cytometry analyses (**D**) of BrdU incorporation of OCI-Ly10 cells bearing the indicated constructs and estimation (in %; **E**) of the fraction of cells in G_1–S–G_2 cell-cycle phases ($n = 4$). BrdU incorporation was monitored after 24 hours of doxycycline stimulation. G_1, S, G_2 cell-cycle phases are indicated in representative flow cytometry analyses. The results are shown as means ± SD. Statistics were performed using two-tailed Student *t* test. *, $P \leq 0.05$; **, $P \leq 0.01$; ***, $P \leq 0.001$. Dox, doxycycline; NS, not significant; NA, not applicable. **F,** GSEA enrichment plots from RNA-seq analyses obtained upon SPI1 WT ($n = 3$) and QE ($n = 3$) expression in OCI-Ly10 cells showing enrichment in QE condition for selected published dataset regarding proliferation, cell cycle, B-cell signaling, and differentiation. The complete lists of significantly enriched gene sets are available in Supplementary Table S15. NES, normalized enrichment score.

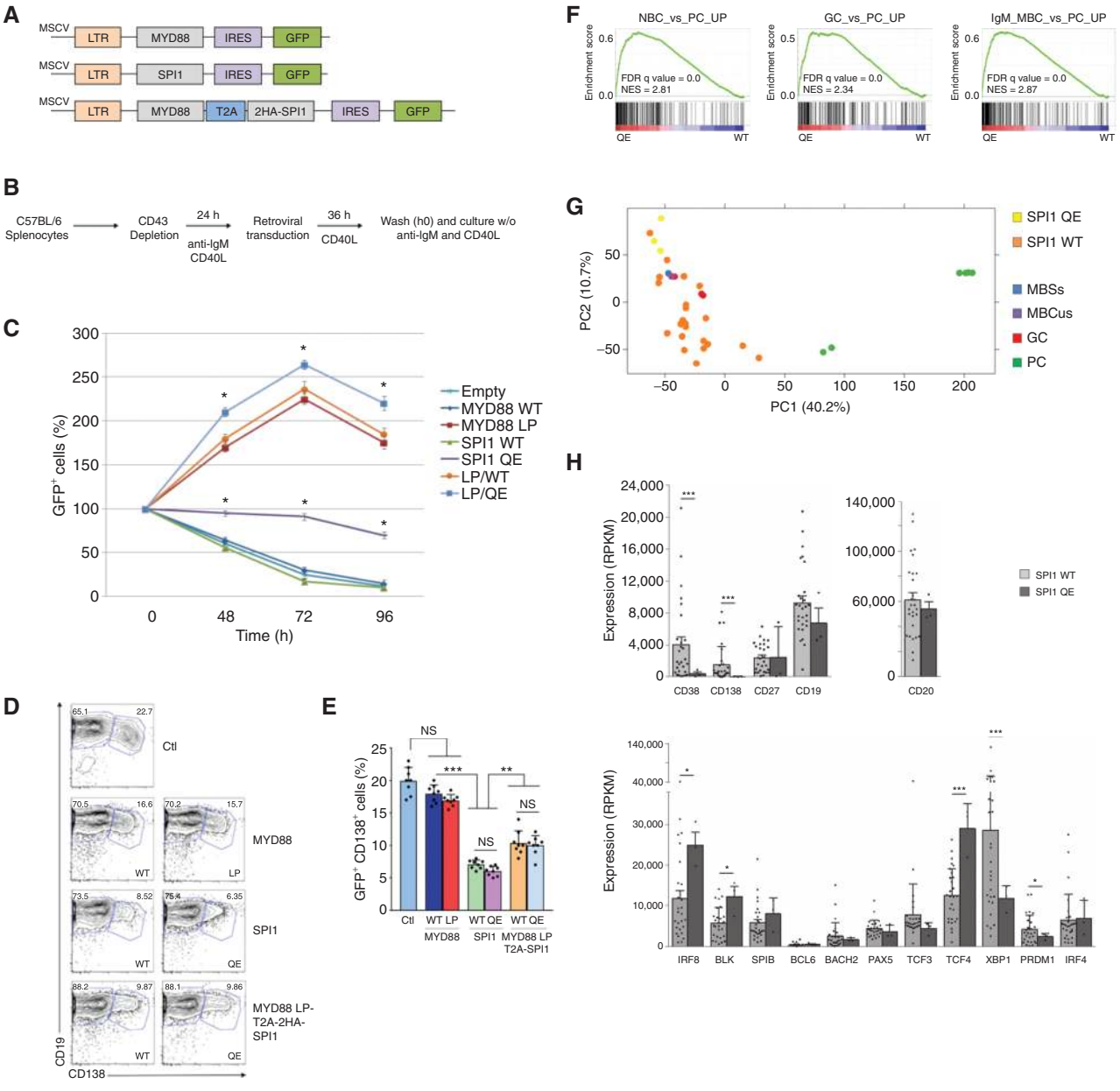

Figure 5. Effects of mutant SPI1 on maturation of murine B cells. **A,** Graphical illustration of MSCV constructs used for murine B-cell experiments. RNA and protein expressions of MYD88 and SPI1 from the different constructs were verified and are illustrated in Supplementary Fig. S7A and S7B. LTR, long terminal repeats sequence; IRES, internal ribosome entry site. **B,** Scheme of murine B-cell experiment. Procedure details are provided in the Methods section. CD40L, CD40 ligand; w/o, without. **C,** Time course of the abundance of GFP$^+$ murine B cells transduced with empty (control) or the color-coded indicated MSCV plasmids [turquoise, empty; blue, MYD88 WT; red, MYD88LP; green, SPI1 WT; violet, SPI1 QE; orange, MYD88LP/SPI1 WT (LP/WT); light blue, MYD88LP/SPI1 QE (LP/QE)] and cultured for 96 hours without any mitogen agent. Results are represented relative to those of GFP$^+$ cells at time 0, set as 100%. Data are representative of three independent experiments ($n = 8$, mean ± SD). Error bars, SD. Statistics were performed using Student *t* test. The LP/QE condition was statistically different from the MYD88LP and LP/WT conditions, whereas SPI1 QE was different from MYD88 WT, SPI1 WT, and empty conditions. *, $P \le 0.05$. LP, L265P. **D,** Representative flow cytometry analyses of CD19$^+$CD138$^+$ cells after 72 hours of culture. CD19 and CD138 expression analysis is gated on viable (Sytox$^-$) transduced (GFP$^+$) cells. **E,** Percentages of CD19$^+$CD138$^+$ GFP$^+$ cells as means ± SD ($n = 8$) are shown in histograms for each construct. **, $P \le 0.01$; ***, $P \le 0.001$. NS, not significant. **F,** GSEA enrichment plots for immunologic signatures using MSigDB, comparing *SPI1* WT ($n = 29$) versus QE ($n = 3$) WM RNA-seq samples. The complete list is available in Supplementary Table S16. MBC, memory B cells; NBC, naïve B cells; PC, plasma cells; NES, normalized enrichment score. **G,** Principal component analysis of normal B cells and WM samples. This analysis included plasma cells (PC; green; $n = 6$), switched (MBCs; blue; $n = 1$) and unswitched (MBCus; violet; $n = 1$) memory, germinal center (GC; red; $n = 3$) B cells, and *SPI1* WT (orange; $n = 29$) and QE (yellow; $n = 3$) WM samples. **H,** Expression of key genes controlling normal B-cell differentiation in *SPI1* WT (light gray; $n = 29$) and QE (dark gray; $n = 3$) WM RNA-seq samples. Error bars, SD. Statistics were performed using Student *t* test. *, $P \le 0.05$; ***, $P \le 0.001$.

WM samples, we performed GSEA of RNA-seq data specifically for immunologic signatures comparing *SPI1* WT ($n = 29$) and QE ($n = 3$) WM samples with available RNA (Supplementary Table S16). The top hit was a gene set comparing naïve B cells to plasma cells (Fig. 5F). The prevalence of this signature was further exemplified by 7 of the top 20 most enriched gene sets (out of more than 4,000 total gene sets) that represent a comparison of plasma cells with either naïve B cells, GC or memory B cells. We then compared transcription profiles between these WM samples and normal B cells representing various steps of differentiation. Using principal component analyses (PCA), normal B-cell samples appeared to spread according to differentiation along the first principal component (PC1), with immature B cells on the left and mature, differentiated plasma cells on the right-hand side (Fig. 5G). Most of the WM samples were located between those two groups in keeping with the blocked plasmablast differentiation step of these tumor cells. Four WM samples and the three *SPI1* QE samples located left of memory B cells, suggesting an earlier arrest of differentiation. Specific examination of cell surface markers and key genes controlling germinal center reaction or plasma cell development confirmed that the *SPI1* QE samples were less differentiated than the other WM samples (Fig. 5H). We observed similar results when we compared *SPI1* QE samples along with the four WM samples, which segregated with them in PCA, with the rest of the cohort (Supplementary Fig. S8A). These observations are in keeping with a lower expression of CD138 in *SPI1* QE bone marrow biopsy WM samples (Fig. 1E; Supplementary Fig. S2A and S2B).

Proliferation of SPI1 QE–Expressing Cells Is Sensitive to JQ1 and Lenalidomide

To support our findings, we extended GSEA using other MSigDB and Lymphochip signatures and compared model cell lines and primary samples data. We confirmed in both settings significant enrichment in classes I/IIa ETS motifs and signaling pathways related to proliferation and BCR and other intracellular signaling (MYC, JAK/STAT, PI3K/AKT, TLR, CD40; Fig. 6A). Most of these enrichments were also confirmed when we performed GSEA considering only genes bound by SPI1 in OCI-Ly10 active promoters' regions (Supplementary Fig. S9A–S9C). Comparison of gene-expression signatures related to ETS1, ELK1, GABPA, and SPI1 showed enrichment in SPI1 QE–expressing samples and cell lines, with respect to WT samples. Lists of genes specifically bound by class I/IIa ETS factors were obtained from ChIP-seq data from GM12878 (Supplementary Table S17) and used in GSEA. Analyses confirmed greater ELK1 and ETS1 than GABPA signature enrichment in mutant samples (Fig. 6B). Note that a SPI1 signature is also enriched in SPI1 QE patients (Fig. 6B).

Signatures of MYC targets were among the most enriched signatures in SPI1 QE–expressing OCI-Ly10 cells and SPI1 QE WM samples (Fig. 6A). We thus interrogated whether SPI1 QE–expressing OCI-Ly10 cells would be sensitive to JQ1, a BET inhibitor which targets MYC, among other activities. As described previously (24), JQ1 treatment induced significant cell death in OCI-Ly10 cells from 48 hours of exposition (data not shown). Although increasing concentrations of JQ1 did not affect viability of control cells at 24 hours, the proportion of viable SPI1 WT- and QE-expressing OCI-Ly10 cells decreased with a significantly more pronounced effect in SPI1 QE condition (Fig. 6C). We confirmed that JQ1 treatment lowered MYC expression in this context (data not shown).

Because of its promising clinical effects and its targeting of IRF4 (25) among other activities, we evaluated the impact of lenalidomide on cell growth. Lenalidomide treatment of cell lines revealed a higher sensitivity of SPI1 QE, with respect to SPI1 WT–expressing cells (Fig. 6D). Expression of *IRF4*-targeting shRNAs (sh*IRF4*-1 and sh*IRF4-2*) in OCI-Ly10 cells resulted in 25% to 28% and 28% to 50% knockdown in, respectively, SPI1 WT- and QE-expressing cells at the IRF4 RNA level, and in an approximate 70% drop in IRF4 protein for both shRNAs in both SPI1 WT- and QE-expressing cells (Supplementary Fig. S10A and S10B). IRF4 knockdown also blunted the proliferative stimulation induced by SPI1 QE (Fig. 6E), confirming a role of IRF4 in SPI1 QE consequences.

We also investigated JQ1 and lenalidomide treatments in BCWM.1 and MWCL-1 cells, which resulted in qualitatively similar differences between SPI1 QE- and WT-overexpressing cells (Fig. 6F–I).

DISCUSSION

We defined the somatic mutation landscape of WM, a rare mature B-cell lymphoproliferative disorder. In addition to confirming recurrent mutations in *MYD88, CXCR4, ARID1A,* and *CD79B*, we identified a novel recurrent somatic mutation (c.676C>G, p.Q226E) in the DNA-binding domain of SPI1, a transcription factor of the class III subgroup of the ETS family. Q226 is present in class III proteins and responsible for the binding of a G at position -2 of the ETS-core GGA(A/T) motif, whereas the E, in classes I and IIa proteins, binds to C at position -2 (17). The mutation modifies the DNA-binding specificity of the protein in promoting binding to DNA recognition sequences of other classes (I and IIa) of ETS proteins. As a result, the mutant SPI1 switches from a WT pattern of chromatin binding (sites preferentially located in enhancers and only 5%–15% in promoters) to a class I/IIa type profile, with binding sites more frequently located in promoters (40%–60%; refs. 26, 27). Our data also show a significant transcriptional enrichment of classes I/IIa ETS target genes in a model cell line and in patient samples expressing SPI1 QE compared with WT.

An important feature of classes I/IIa ETS factors is that DNA binding and transcription activities are tightly regulated by intracellular signaling pathways, such as calcium and MAPK activity (28, 29), suggesting that promoters bound by the SPI1 QE may escape normal regulation. Indeed, overexpression of SPI1 QE was associated with growth stimulation with respect to the SPI1 WT in all tested cell lines. Mutant SPI1 expression was associated with enrichment in transcription signatures related to cell cycle, proliferation, intracellular signaling pathways, and also MYC- and IRF4-related transcriptional programs. As SPI1 interaction with transcription factors (30) and epigenetic regulators, such as CBP (31) and TET2 (32), is important for their regulation,

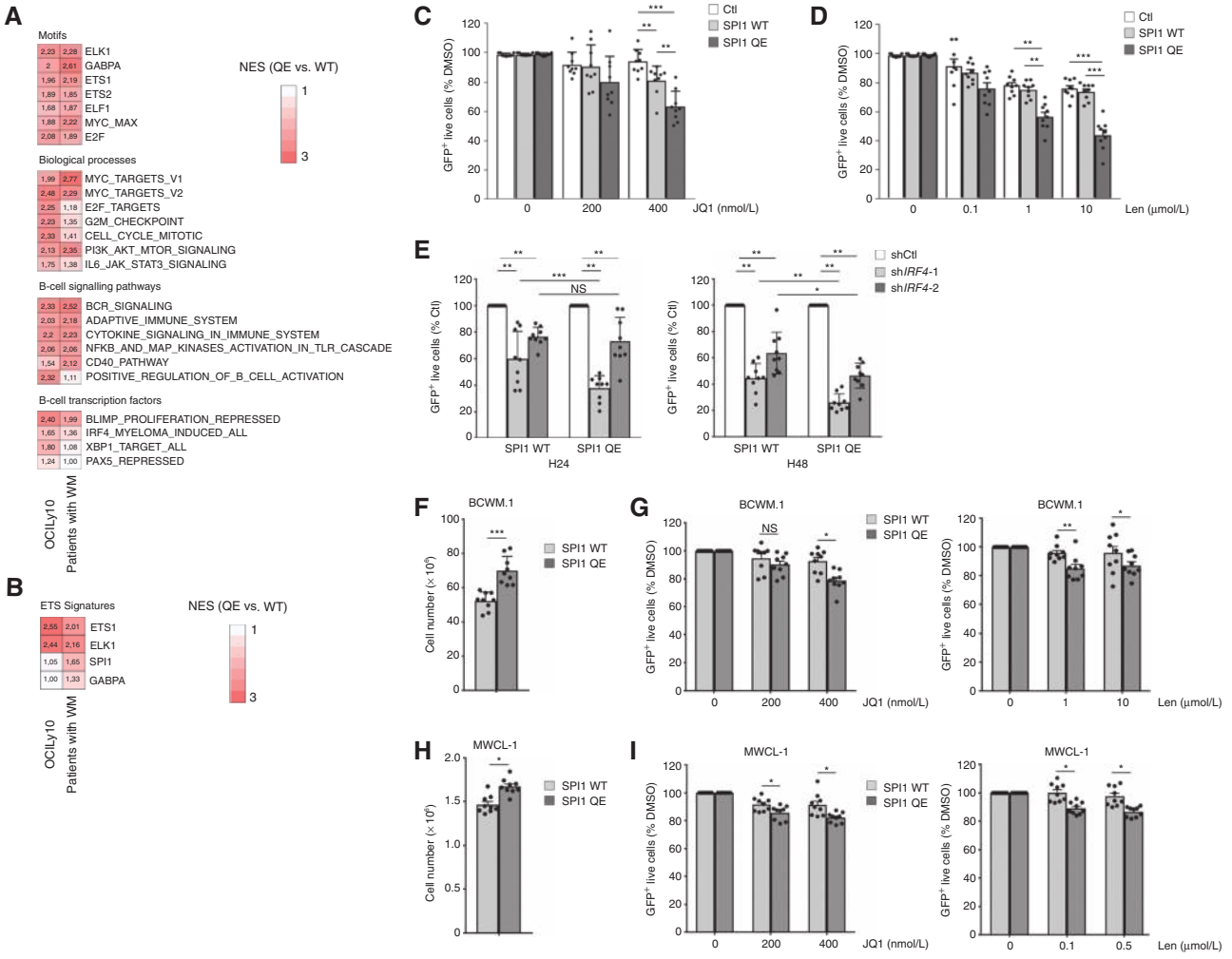

Figure 6. Genes and pathways activated by mutant SPI1 may be targeted. **A,** Integration of GSEA in OCI-Ly10 cells and WM cases, comparing SPI1 QE to WT RNA-seq samples, using MSigDB and the Lymphochip databases. Heat map represents the normalized enrichment score (NES) of each gene set signature tested. Only pathways relevant to transcription factor motifs, intracellular signaling pathways, and B-cell biology are shown in the figure. The complete lists are available in Supplementary Tables S15 and S16. NES values are indicated inside each box. **B,** GSEA of ETS1, ELK1, GABPA, and SPI1-specific signatures in SPI1 QE and WT OCI-Ly10 (left) and WM (right) samples. These specific signatures were generated from ENCODE ChIP-seq data of GM12878. Heat map represents the NES of each gene set signature tested. Represented signatures are enriched in SPI1 QE samples. NES values are indicated inside each box. **C,** The BET inhibitor JQ1 decreases cellular proliferation of SPI1 QE–transduced OCI-Ly10 cells. Viability of OCI-Ly10 cells bearing empty (Ctl; white), SPI1 WT (light gray), or QE (dark gray) constructs ($n = 9$, mean ± D). OCI-Ly10 cells were treated for 24 hours with doxycycline and the indicated concentrations of BET inhibitor (JQ1). Cell viabilities are represented relative to those without JQ1 treatment. Three independent experiments have been performed. NS, not significant. **, $P \leq 0.01$; ***, $P \leq 0.001$. Statistics were performed using two-tailed Student *t* test. Error bars, SD. **D,** SPI1 QE–expressing OCI-Ly10 cells are more sensitive to lenalidomide (Len) than those expressing SPI1 WT. Viability of OCI-Ly10 cells bearing empty (Ctl; white), SPI1 WT (light gray), or QE (dark gray) constructs ($n = 9$, mean ± SD). OCI-Ly10 cells were treated for 24 hours with doxycycline and the indicated concentrations of lenalidomide. Cell viabilities are represented relative to those without lenalidomide treatment. Three independent experiments have been performed. **, $P \leq 0.01$; ***, $P \leq 0.001$. Statistics were performed using two-tailed Student *t* test. Error bars, SD. **E,** SPI1 QE–expressing OCI-Ly10 cells are more sensitive than those expressing SPI1 WT to shRNAs targeting IRF4. Viability of OCI-Ly10 cells transduced with puromycin-inducible shRNAs [one control (Ctl; white) and two targeting IRF4 (sh*IRF4*-1, light gray; sh*IRF4*-2, dark gray; $n = 9$, mean ± SD)]. OCI-Ly10 cells were treated for 24 hours (left) or 48 hours (right) with puromycin. Cell viabilities are represented relative to those of control shRNA. Three independent experiments have been performed. NS, not significant. *, $P \leq 0.05$; **, $P \leq 0.01$; ***, $P \leq 0.001$. Statistics were performed using two-tailed Student *t* test. Error bars, SD. **F–I,** Overexpression of SPI1 WT and QE proteins in WM-related cell lines (BCWM.1 and MWCL-1). SPI1 QE–expressing cells grow more and are more sensitive to JQ1 and lenalidomide (Len) treatment than those expressing SPI1 WT. **F,** Quantitation of *in vitro* proliferation of BCWM.1-transduced cells expressing either SPI1 WT (light gray) or QE (dark gray; $n = 9$, mean ± SD). **G,** Viability of BCWM.1 cells bearing SPI1 WT (light gray) or QE (dark gray) constructs ($n = 9$, mean ± SD) when treated with the indicated concentration of JQ1 (left) or lenalidomide (right). **H,** Quantitation of *in vitro* proliferation of MWCL-1–transduced cells expressing either SPI1 WT (light gray) or QE (dark gray; $n = 9$, mean ± SD). **I,** Viability of MWCL-1 cells bearing SPI1 WT (light gray) or QE (dark gray) constructs ($n = 9$, mean ± SD) when treated with the indicated concentration of JQ1 (left) or lenalidomide (right). The levels of SPI1 proteins were checked (Supplementary Fig. S5A–S5D) and found to be equivalent for SPI1 WT and QE conditions. Cell viabilities are represented relative to those without JQ1 or lenalidomide treatment. Three independent experiments have been performed in triplicate. Statistics were performed using two-tailed Student *t* test. Error bars, SD. NS, not significant. *, $P \leq 0.05$; **, $P \leq 0.01$; ***, $P \leq 0.001$.

the impact of *SPI1* QE mutation on these activities will have to be investigated.

Missense mutations in transcription factor genes in hematopoietic malignancies, such as those of *ELF4, EGR2, MEF2C,* or *IRF4* in mature B-cell disorders (15, 33, 34), may affect the DNA binding of the protein. Together with the recent description of missense mutations modifying the DNA-binding properties of Krüppel-like factor 5 gene (*KLF5*; ref. 35), our work provides a framework for understanding the functional consequences of missense mutations.

Oncogenic properties of ETS proteins have been largely described in solid tumors. Rearrangements of ETS loci are a hallmark of prostate cancer with around half of tumors showing alterations at an ETS gene locus (36). However, abnormalities of ETS proteins have rarely been identified in mature B-cell malignancies, with the exception of *ELF4* mutations in chronic lymphocytic leukemia (33), translocations involving *SPIB*, and gain of chromosome 11q24, encompassing *ETS1* and *FLI1*, in diffuse large B-cell lymphoma (DLBCL; refs. 37, 38).

Various members of the ETS family also regulate B-cell differentiation and function. In murine models, the roles of six ETS proteins have been studied in detail in B-lymphocytes, including ETS1 (2, 27), FLI1 (39), GABPA (40), and the three class III factors SPI1, SPIB, and SPIC (41). Survey of their expression during human and murine B-cell maturation suggest the highest activity of the class I/IIa ETS factors in GC B cells, together with the highest level of ETS1 transcription (Supplementary Fig. S8B–S8E).

Loss of ETS1 leads to premature B-cell differentiation into antibody-secreting cells (42), and recent reports have emphasized that SPI1 and SPIB physiologically act as negative regulators of plasma cell development and sensors to environmental stimuli (8, 9, 43). Considering that WM is characterized by a differentiation block at the transition from post-GC lymphocyte to plasma cell, we confirmed the impact of *SPI1* mutations on terminal B-cell differentiation. Indeed, SPI1-expressing B cells demonstrated less efficient plasma cell differentiation in an *in vitro* model. Moreover, our gene-expression analyses revealed that mutated *SPI1* WM cases were less differentiated than the other WM samples. Additional analyses will be required to comprehensively characterize the relationship between the different classes of ETS in the different steps of B-cell differentiation and in the differentiation blockade observed in WM. In this regard, it is worth noting that GSEA of RNA-seq from normal B-cell populations shows a significant enrichment of classes I/IIa motifs in naïve, GC, or memory B-cell populations versus plasma cells (Supplementary Fig. S9D–S9I). It also remains to be shown whether other missense mutations in genes of ETS family (*ETS1, ELK1*) or transcription factors (*EGR1, EGR2, MEF2C*; refs. 15, 34) identified in other B-cell lymphoproliferative disorders may have the same impact on DNA recognition and B-cell differentiation.

Finally, *SPI1* Q226E mutations are associated with poor prognosis, although impact on survival needs to be validated. The enrichment of MYC pathway associated with SPI1 Q226E–expressing cases is of interest, as BET inhibitors target this pathway and may be of therapeutic benefit in these high-risk patients. Similarly, *in vitro* experiments show that cells expressing SPI1 Q226E are sensitive to lenalidomide, which is also known to indirectly target the important B-lymphocyte transcription factors. Our results thus identify mutant SPI1 as a new genetic biomarker for patients with poor-prognosis WM and point to treatment options for this patient group.

METHODS

Detailed materials and methods are available in the Supplementary Data.

Patients and Materials

A total of 85 patients meeting the diagnostic criteria for WM (44), were enrolled in this study. Written informed consent for bone marrow and biological analyses were obtained from all patients in accordance with the Declaration of Helsinki and with ethical approval from the local ethics committee (CPP Ile-De-France 05/21/2014). Characteristics of this cohort are summarized in Supplementary Table S1. Cytogenetic analyses were performed as described previously (45). Samples from patients with DLBCL (n = 147), follicular lymphoma (n = 56), marginal zone lymphoma (n = 12), and mantle-cell lymphoma (n = 19), were obtained with their informed consent and the approval of the local Research Ethics Committees (Gustave Roussy, Centre Henri Becquerel, Pitié-Salpêtrière, and Cochin hospitals). Patients with chronic lymphocytic leukemia (n = 360) were enrolled in two clinical trials (www.ClinicalTrials.gov; NCT00564512 and NCT00645606). Primer sequences are available upon request.

Statistical Analysis

Data are depicted as mean ± SD. P values were calculated with the two-tailed unpaired Student t test unless otherwise specified. All statistical analyses were performed with Prism software version 6.0 (GraphPad Software, Inc.).

Clinical and laboratory variables were compared across patients with or without mutation using the Wilcoxon rank-sum test (for quantitative variables) or the Fisher exact test (for qualitative variables). Time-to-treatment (time between diagnosis and first treatment) was compared across groups using log-rank tests. For overall survival (survival since study enrollment) a Kaplan–Meier estimator was used and survival curves were compared using the log-rank test. All tests were two-sided, with P value less than 0.05 considered statistically significant. Softwares were SAS 9.3 (SAS, Inc.) and R 3.0.2.

Cell Sorting and Nucleic Acid Extraction

Samples were processed as described previously (34). Tumor cells were defined by CD19 and monotypic light chain positivity. Controls were matched $CD3^+$ T cells. The cellular populations were sorted using an Influx Cell Sorter (BD Biosciences). Sorted cells were subjected to an additional round of sorting to reach purity over 98%. Nucleic acids were extracted using the AllPrep DNA/RNA Kit (Qiagen).

Sequencing

Whole-exome sequencing (WES) was conducted on paired samples from 16 patients as described previously (34). Library was built with SureSelect All Exon Kit (Agilent Technologies). Sequences were analyzed as described previously (34) with minor modifications (Supplementary Methods; Supplementary Tables S2 and S3; Supplementary Fig. S1A–S1C).

Twenty recurrently mutated genes from our WES cohort or in the literature were selected for targeted sequencing of an extended series of WM samples using Ion AmpliSeq Designer (Thermo Fisher

Scientific). See Supplementary Table S4 for genomic coordinates of targeted regions and Supplementary Fig. S1D for the list of genes. Accession numbers for sequence data are E-MTAB-7881, E-MTAB-7882, and EGAS00001003603.

RNA-seq

RNA-seq was performed and analyzed as described previously (refs. 34, 46; see also Supplementary Material). Molecular pathway analysis and GSEA were performed using GSEA (2.2.3), the Molecular Signatures Database (6.2, Broad Institute) and the Lymphoid Signature Database (21). Comparison with normal B-cell differentiation expression profiles was performed using Blueprint data (accession numbers: EGAD00001002347, EGAD00001002414, EGAD00001001164, EGAD00001002452, EGAD00001002323, EGAD00001002476).

qPCR Analyses

CDNA was generated using SuperScript IV Reverse Transcriptase (Invitrogen). TaqMan probes were purchased from Applied Biosystems: ABL1 (Hs1104728), GUSB (Hs00939627), IRF4 (Hs01056533), MYC (Hs00905030). The expression level of each gene was assessed by qRT-PCR with ABI Prism 7500 and calculated following the $\Delta\Delta C_t$ method. Each sample was analyzed in triplicate and normalized to ABL1 or GUSB expression as indicated.

Cell Culture and Drugs

All cell lines were maintained in standard conditions and verified for known molecular features (described in Supplementary Fig. S11A–S11C). OCI-Ly10 cells were a kind gift from K. Leroy (Institut Cochin, Paris, France). BCWM.1 and MWCL-1 cells were a kind gift from R. Guièze and R. Lemal (CHU Clermont-Ferrand, France). OCI-Ly10, BCWM.1, and MWCL-1 cells were negative for *SPI1* Q226E mutation (Supplementary Fig. S11A). Ba/F3 cells were a kind gift from P. Dubreuil (CRCM, Marseille, France) and were supplemented with 1 ng/mL of rmIL3. The BET inhibitor JQ1 was a kind gift from J. Bradner (Dana-Farber Cancer Institute, Boston, MA). Lenalidomide was purchased from Aldrich Chemistry (reference CDS022536).

Vectors, Retroviral and Lentiviral Production, Transduction, and Transplantation

SPI1 (NM_003120.2), *MYD88* (NM_002468.4), and derivative cDNAs were subcloned into murine stem cell virus (MSCV)-IRES-GFP, pV81, or pcDNA3. Mutations were introduced using the Quick Change site-directed Mutagenesis Kit (Agilent) or by PCR. Every PCR-amplified or mutagenized fragment was sequence-checked. Viral particles, transduction procedures, bone marrow transplantation assays, and hematopoietic differentiation analyses were performed as described previously (47, 48).

Cells were transduced with WT or mutated pV81/GFP-SPI1 viruses and flow-sorted twice gating on viable GFP$^+$ cells 24 hours after doxycycline addition (1,000 ng/mL; Sigma, reference D-9891) to reach more than 90% of GFP$^+$ cells. These flow-sorted cells were used for subsequent analyses. Both mutant and WT proteins were expressed at similar levels (Supplementary Fig. S4B and S5A–5D). Cells transduced by lentivirus containing shRNA targeting human IRF4 [TRCN0000014765 (sh*IRF4*-1) and TRCN000014767 (sh*IRF4*-2; Sigma)] were grown 3 days in puromycin (1,000 ng/mL) for selection.

EMSA

The SPI1 core-binding sites GGAA boxes (in bold) and have been described previously (5′GA**GGAA**CCGCGGAATCA**GGAA**GAACTG GCCGGCGC3′; ref. 18). EMSA was performed using nonradioactive reagents, as described in Supplementary Methods. Three independent experiments were performed.

Isothermal Calorimetric Assay

Interactions between the WT or mutant DNA-binding domains of SPI1 fused to GST (49) and DNA containing "lambda B1," a classic SPI1-binding site (19), and mutants thereof, were analyzed using a VP-ITC calorimeter (Microcal). Prior to measurements, all solutions were degassed under vacuum. The reaction cell was loaded with GST-DBD WT or QE and the syringe was filled with 20mer DNA substrates containing the SPI1-binding site. The lambda B1–derived sequences used as probes were as follows: WT, TAAAA**GGAA** GTGAAACCAAG; mutant same as WT, with a mutant sequence, TAAAA<u>CC</u>**AA**GTGAAACCAAG; ETS1-like same as WT with an ETS1-like sequence, TAA<u>CC</u>**GGAA**GTGAAACCAAG. The proteins were extensively dialyzed against the buffer (25 mmol/L Na phosphate pH 8.0, 150 mmol/L NaCl, 5 mmol/L β-mercaptoethanol). K_d were obtained by nonlinear least-squares fitting of the experimental data using the single set of independent binding sites model of the Origin software provided with the instrument. All binding experiments were performed in duplicate or triplicate at 25°C.

Luciferase Assay

HEK293T cells were transiently transfected with equimolar amounts of empty pcDNA3 vector (control, ctl), pcDNA3 vectors encoding WT or mutant SPI1, along with modified firefly luciferase reporter constructs and a *Renilla* luciferase control reporter. Cells were harvested 24 hours after transfection and the Dual Luciferase Reporter Assay (Promega) was used for detecting luciferase activity. A minimum of three independent experiments in optimized conditions were performed. Checking for protein expression indicated that the mutant protein was consistently overexpressed with respect to the WT protein. Quantifying protein expression of over 5 Western blots (3 of them are shown in Supplementary Fig. S3I–S3K) indicated an average 1.5 times stronger SPI1 protein expression in SPI1 QE over WT. Activity was normalized with respect to protein quantity and to *Renilla* activity from a cotransfected vector. Reporters used were Fes (18), lambda B1 (19), and GPAA1 sequences (3 copies) fused to the TK promoter. Sequences were as follows: Fes, GA**GGAA**CCGC **GGAA**TCA**GGAA**GAACTGGCCGGCGC; GPAA1 WT, TGGGACC **GGAA**GTGCGGG; GPAA1 mutant, TGGGACC<u>**CC**</u>**AA**GTGCGGG; lambda B1 WT, TAAAA**GGAA**GTGAAACCAAG; lambda B1 mutant, TAAAA<u>**CC**</u>**AA**GTGAAACCAAG. The core ETS recognition sequence is in bold; mutant bases are underlined.

Cellular Proliferation Assays

Doxycycline (1,000 ng/mL) was added to exponentially growing cells. GFP$^+$ cells were flow-sorted after 24 hours and plated in triplicate in 48-well plates, 90,000 cells/well, in 300 μL of media containing doxycycline (1,000 ng/mL). The time of flow-sorting was considered to be "hour 0" (H0). The number of viable cells was determined by counts of Trypan blue–negative cells and the percentage of viable (Sytox) GFP$^+$ cells was checked by flow cytometry at H48. Two independent experiments were performed in triplicate. Transduced BCWM.1 and MWCL-1 cells were analyzed similarly, in adapted culture conditions (75,000 or 150,000 cells/wells, respectively, in a 24-well plate). Three independent experiments were performed in triplicate.

Drug-Sensitivity Assays

OCI-Ly10 transduced cells were seeded at 300,000 cells/mL in triplicate in 300 μL of fresh media, in a 48-well plate. JQ1 and lenalidomide were dissolved in DMSO and equal volumes were added to cells to reach the indicated final concentrations. OCI-Ly10 transduced cells were treated with doxycycline (1,000 ng/mL) and the indicated concentrations of JQ1 or lenalidomide for, respectively, 24 hours and 48 hours. Doxycycline, JQ1, and lenalidomide were added to the media at the same time (H0). BCWM.1 and MWCL-1 transduced cells were

seeded at 150,000 or 250,000 cells/well, respectively, in 500 μL of fresh media, and analyzed similarly. Cell numbers were estimated as described above. Three independent experiments were performed in triplicate.

Flow Cytometry and Cell-Cycle Analyses

Cells analyzed by flow cytometry were stained in PBS 1× supplemented with 2% FBS for 30 minutes at 4°C with washing prior to FACS analysis. Antibodies were purchased from Becton Dickinson or eBioscience for human (h) and murine (m) antibodies. Viability of cells was confirmed by using the Sytox Blue (Invitrogen) viability marker. Cells were analyzed on a FACS CantoII with FACS Diva Software (BD Biosciences). For cell-cycle analyses, cells were fixed in 70% cold ethanol and stained with propidium iodide and 7-AAD. Quantification of different cycle phases was performed using Watson Pragmatic Algorithm (FlowJo). Alternatively, cells were labeled by the addition of 10 mmol/L BrdU (5-bromodeoxyuridine) to the culture medium for 1 hour before harvest. BrdU and 7-AAD were detected with the APC BrdU Detection Kit (BD Biosciences). Stained cells were analyzed with a FACS Canto II (BD Biosciences) and data analyses were performed with FlowJo 9.5.2 Software (TreeStar).

Chromatin Immunoprecipitation, Sequencing, and Analysis

ChIP protocol, adapted from the MagnaChIP Kit Protocol (Millipore) and ref. 50, and analyses are detailed in the Supplementary Material. ChIP-seq data for ELK1 (ENCFF556JBS), ETS1 (ENCFF-332PGQ), GABPA (ENCFF116EXQ), and SPI1 (ENCFF002CHQ) in the GM12878 cell line were obtained from ENCODE. The first 500 peaks, unique to the transcription factor with the highest P_{adj} (as determined by HOMER merge peaks, v4.10.3), were selected and attributed to the nearest gene. Genes unique to a transcription factor were then identified (Supplementary Table S17) and used in GSEA.

Murine B-cell Transduction and Culture

All experiments were performed on 8- to 10-week-old C57BL/6 mice (The Jackson Laboratory) and procedures conformed to ethical principles and guidelines revised and approved by the Animal Care Committee of Gustave Roussy. Red cells were lysed from splenic suspensions for 5 minutes at 4°C. After washing (PBS 1×; 2% FBS), $CD43^-$ cells were separated using AutoMACS Pro Separator Instrument (Miltenyi Biotec) with anti-CD43 antibody–coated magnetic beads and comprised more than 95% $B220^+$ cells (Supplementary Fig. S7C). $CD43^-$ cells were activated with anti-IgM (7 μg/mL) and anti-CD40 (10 μg/mL) for 24 hours before retroviral transduction. Transduced B cells were then cultured in media containing anti-CD40 (10 μg/mL). The number of viable cells was determined by counts of Trypan blue–negative cells and the percentage of GFP^+ $Sytox^-$ cells was determined by flow cytometry. Transduced cells were washed and seeded at 1×10^6 cells/mL in fresh complete RPMI without any mitogen supplement. The start of the mitogen-free cultures was designated as "H0." The number of GFP^+ cells was monitored by counting Trypan blue–negative cells and by flow cytometry.

Disclosure of Potential Conflicts of Interest

F. Damm reports receiving a commercial research grant from Novartis. E. Verhoeyen has ownership interest in a patent covering the BAEV glycoprotein pseudotyped lentiviral vectors for transduction of human B cells, T cells, and hematopoietic stem cells. V. Leblond has received speakers bureau honoraria from Roche, Janssen, Gilead, AbbVie, and Amgen, and is a consultant/advisory board member for AstraZeneca, Janssen, and Roche. V. Ribrag reports receiving commercial research grants from Servier and ArgenX; has received speakers bureau honoraria from Infinity, BMS, Pharmamar, NanoString, MSD, Roche, Gilead, Incyte, and Epizyme; and is a consultant/advisory board member for Servier. P. Morel is a consultant/advisory board member for Janssen. P. Vyas reports receiving a commercial research grant from Celgene; has received speakers bureau honoraria from Celgene, Pfizer, Jazz, Astellas, Daiichi Sankyo, and Novartis; and has ownership interest (including stocks and patents) in Oxstem Oncology. No potential conflicts of interest were disclosed by the other authors.

Authors' Contributions

Conception and design: D. Roos-Weil, F. Nguyen-Khac, O.A. Bernard
Development of methodology: D. Roos-Weil, V. Della-Valle, H. Ghamlouch, C. Hérate, E. Mylonas, F.-L. Cosset, E. Verhoeyen, P. Vyas, T. Mercher, S. Aoufouchi, N. Droin, C. Guillouf, F. Nguyen-Khac
Acquisition of data (provided animals, acquired and managed patients, provided facilities, etc.): D. Roos-Weil, C. Decaudin, M. Armand, V. Della-Valle, H. Ghamlouch, V. Ropars, C. Hérate, D. Lara, E. Durot, R. Haddad, E. Mylonas, F. Damm, F. Pflumio, B. Stoilova, M. Metzner, V. Camara-Clayette, F.-L. Cosset, V. Leblond, V. Ribrag, P. Cornillet-Lefebvre, P. Rameau, N. Azar, F. Charlotte, P. Morel, J.-B. Charbonnier, P. Vyas, T. Mercher, N. Droin, C. Guillouf, F. Nguyen-Khac
Analysis and interpretation of data (e.g., statistical analysis, biostatistics, computational analysis): D. Roos-Weil, V. Della-Valle, M.K. Diop, H. Ghamlouch, V. Ropars, C. Hérate, D. Lara, E. Mylonas, O. Elemento, P. Dessen, V. Ribrag, F. Charlotte, J.-B. Charbonnier, P. Vyas, T. Mercher, N. Droin, C. Guillouf, F. Nguyen-Khac, O.A. Bernard
Writing, review, and/or revision of the manuscript: D. Roos-Weil, V. Della-Valle, M.K. Diop, D. Lara, E. Durot, E. Mylonas, F. Damm, B. Stoilova, E. Verhoeyen, V. Leblond, V. Ribrag, P. Cornillet-Lefebvre, N. Azar, F. Charlotte, P. Morel, J.-B. Charbonnier, P. Vyas, T. Mercher, S. Aoufouchi, N. Droin, C. Guillouf, F. Nguyen-Khac, O.A. Bernard
Administrative, technical, or material support (i.e., reporting or organizing data, constructing databases): C. Guillouf
Study supervision: D. Roos-Weil, P. Vyas, F. Nguyen-Khac, O.A. Bernard

Acknowledgments

We thank the members of the Gustave Roussy platforms, including Patrick Gonin for excellent mouse care, Yann Lecluse for flow cytometry, Xavier Veaute and the CIGEX facility for protein production, and Patricia Kannouche for helpful discussions. We thank the Blueprint consortium for access to RNA-seq data, the Encode consortium for some ChIP-seq data, and W. Cook (La Trobe University, Melbourne, Australia) and R. DeKoter (Western University in London, Ontario) for cell lines. This work was supported by grants from INSERM, Institut National du Cancer (INCa), 2013-PLBIO-09, 2016-PLBIO-068, JTC 2014-143, INCa-DGOS-INSERM_12551, INCA-DGOS-Inserm_12560, Association Laurette Fugain (to O.A. Bernard and F. Nguyen-Khac), LNCC, Comité Val-d'Oise de la Ligue contre le cancer, infrastructure FRISBI ANR-10-INBS-05, Fondation ARC (SFI20111203530), GEFLUC, and FILO. P. Vyas acknowledges funding from the MRC Disease Team Awards (G1000729/94931 and MR/L008963/1), MRC Molecular Haematology Unit and the Oxford Partnership Comprehensive Biomedical Research Centre (NIHR BRC Funding scheme.oxfbrc-2012-1). H. Ghamlouch is a recipient of successive grants from région Ile de France and Fondation de France (No 00067113). C. Hérate, D. Lara, and E. Durot were recipients of fellowships from region Ile de France, Fondation pour la Recherche Médicale, and Fondation ARC, respectively.

The costs of publication of this article were defrayed in part by the payment of page charges. This article must therefore be hereby marked *advertisement* in accordance with 18 U.S.C. Section 1734 solely to indicate this fact.

Received August 1, 2018; revised March 28, 2019; accepted April 18, 2019; published first April 24, 2019.

REFERENCES

1. Basso K, Dalla-Favera R. Germinal centres and B cell lymphomagenesis. Nat Rev Immunol 2015;15:172–84.
2. Garrett-Sinha LA.Review of Ets1 structure, function, and roles in immunity. Cell Mol Life Sci 2013;70:3375–90.
3. Sharrocks AD.The ETS-domain transcription factor family. Nat Rev Mol Cell Biol 2001;2:827–37.
4. Hollenhorst PC, McIntosh LP, Graves BJ. Genomic and biochemical insights into the specificity of ETS transcription factors. Annu Rev Biochem 2011;80:437–71.
5. Scott EW, Simon MC, Anastasi J, Singh H. Requirement of transcription factor PU.1 in the development of multiple hematopoietic lineages. Science 1994;265:1573–7.
6. Cook WD, McCaw BJ, Herring C, John DL, Foote SJ, Nutt SL, et al. PU.1 is a suppressor of myeloid leukemia, inactivated in mice by gene deletion and mutation of its DNA binding domain. Blood 2004;104:3437–44.
7. Rosenbauer F, Wagner K, Kutok JL, Iwasaki H, Le Beau MM, Okuno Y, et al. Acute myeloid leukemia induced by graded reduction of a lineage-specific transcription factor, PU.1. Nat Genet 2004;36:624–30.
8. Carotta S, Willis SN, Hasbold J, Inouye M, Pang SH, Emslie D, et al. The transcription factors IRF8 and PU.1 negatively regulate plasma cell differentiation. J Exp Med 2014;211:2169–81.
9. Willis SN, Tellier J, Liao Y, Trezise S, Light A, O'Donnell K, et al. Environmental sensing by mature B cells is controlled by the transcription factors PU.1 and SpiB. Nat Commun 2017;8:1426.
10. Mueller BU, Pabst T, Osato M, Asou N, Johansen LM, Minden MD, et al. Heterozygous PU.1 mutations are associated with acute myeloid leukemia. Blood 2002;100:998–1007.
11. Lavallee VP, Baccelli I, Krosl J, Wilhelm B, Barabe F, Gendron P, et al. The transcriptomic landscape and directed chemical interrogation of MLL-rearranged acute myeloid leukemias. Nat Genet 2015;47:1030–7.
12. Seki M, Kimura S, Isobe T, Yoshida K, Ueno H, Nakajima-Takagi Y, et al. Recurrent SPI1 (PU.1) fusions in high-risk pediatric T cell acute lymphoblastic leukemia. Nat Genet 2017;49:1274–81.
13. Ngo VN, Young RM, Schmitz R, Jhavar S, Xiao W, Lim KH, et al. Oncogenically active MYD88 mutations in human lymphoma. Nature 2011;470:115–9.
14. Treon SP, Xu L, Yang G, Zhou Y, Liu X, Cao Y, et al. MYD88 L265P somatic mutation in Waldenstrom's macroglobulinemia. N Engl J Med 2012;367:826–33.
15. Reddy A, Zhang J, Davis NS, Moffitt AB, Love CL, Waldrop A, et al. Genetic and functional drivers of diffuse large B cell lymphoma. Cell 2017;171:481–94.
16. Morel P, Duhamel A, Gobbi P, Dimopoulos MA, Dhodapkar MV, McCoy J, et al. International prognostic scoring system for Waldenstrom macroglobulinemia. Blood 2009;113:4163–70.
17. Wei GH, Badis G, Berger MF, Kivioja T, Palin K, Enge M, et al. Genome-wide analysis of ETS-family DNA-binding *in vitro* and *in vivo*. EMBO J 2010;29:2147–60.
18. Ray-Gallet D, Mao C, Tavitian A, Moreau-Gachelin F. DNA binding specificities of Spi-1/PU.1 and Spi-B transcription factors and identification of a Spi-1/Spi-B binding site in the c-fes/c-fps promoter. Oncogene 1995;11:303–13.
19. Brass AL, Zhu AQ, Singh H. Assembly requirements of PU.1-Pip (IRF-4) activator complexes: inhibiting function *in vivo* using fused dimers. EMBO J 1999;18:977–91.
20. Ernst J, Kellis M. Chromatin-state discovery and genome annotation with ChromHMM. Nat Protoc 2017;12:2478–92.
21. Shaffer AL, Wright G, Yang L, Powell J, Ngo V, Lamy L, et al. A library of gene expression signatures to illuminate normal and pathological lymphoid biology. Immunol Rev 2006;210:67–85.
22. Laslo P, Pongubala JM, Lancki DW, Singh H. Gene regulatory networks directing myeloid and lymphoid cell fates within the immune system. Semin Immunol 2008;20:228–35.
23. Wang JQ, Jeelall YS, Beutler B, Horikawa K, Goodnow CC. Consequences of the recurrent MYD88(L265P) somatic mutation for B cell tolerance. J Exp Med 2014;211:413–26.
24. Ceribelli M, Kelly PN, Shaffer AL, Wright GW, Xiao W, Yang Y, et al. Blockade of oncogenic IkappaB kinase activity in diffuse large B-cell lymphoma by bromodomain and extraterminal domain protein inhibitors. Proc Natl Acad Sci U S A 2014;111:11365–70.
25. Yang Y, Shaffer AL 3rd, Emre NC, Ceribelli M, Zhang M, Wright G, et al. Exploiting synthetic lethality for the therapy of ABC diffuse large B cell lymphoma. Cancer Cell 2012;21:723–37.
26. Solomon LA, Li SK, Piskorz J, Xu LS, DeKoter RP. Genome-wide comparison of PU.1 and Spi-B binding sites in a mouse B lymphoma cell line. BMC Genomics 2015;16:76.
27. Saelee P, Kearly A, Nutt SL, Garrett-Sinha LA. Genome-wide identification of target genes for the key B cell transcription factor Ets1. Front Immunol 2017;8:383.
28. Cowley DO, Graves BJ. Phosphorylation represses Ets-1 DNA binding by reinforcing autoinhibition. Genes Dev 2000;14:366–76.
29. Foulds CE, Nelson ML, Blaszczak AG, Graves BJ. Ras/mitogen-activated protein kinase signaling activates Ets-1 and Ets-2 by CBP/p300 recruitment. Mol Cell Biol 2004;24:10954–64.
30. Hosokawa H, Ungerback J, Wang X, Matsumoto M, Nakayama KI, Cohen SM, et al. Transcription Factor PU.1 represses and activates gene expression in early T cells by redirecting partner transcription factor binding. Immunity 2018;49:782.
31. Hong W, Kim AY, Ky S, Rakowski C, Seo SB, Chakravarti D, et al. Inhibition of CBP-mediated protein acetylation by the Ets family oncoprotein PU.1. Mol Cell Biol 2002;22:3729–43.
32. de la Rica L, Rodriguez-Ubreva J, Garcia M, Islam AB, Urquiza JM, Hernando H, et al. PU.1 target genes undergo Tet2-coupled demethylation and DNMT3b-mediated methylation in monocyte-to-osteoclast differentiation. Genome Biol 2013;14:R99.
33. Landau DA, Tausch E, Taylor-Weiner AN, Stewart C, Reiter JG, Bahlo J, et al. Mutations driving CLL and their evolution in progression and relapse. Nature 2015;526:525–30.
34. Damm F, Mylonas E, Cosson A, Yoshida K, Della Valle V, Mouly E, et al. Acquired initiating mutations in early hematopoietic cells of CLL patients. Cancer Discov 2014;4:1088–101.
35. Zhang X, Choi PS, Francis JM, Gao GF, Campbell JD, Ramachandran A, et al. Somatic superenhancer duplications and hotspot mutations lead to oncogenic activation of the KLF5 transcription factor. Cancer Discov 2018;8:108–25.
36. Tomlins SA, Rhodes DR, Perner S, Dhanasekaran SM, Mehra R, Sun XW, et al. Recurrent fusion of TMPRSS2 and ETS transcription factor genes in prostate cancer. Science 2005;310:644–8.
37. Lenz G, Nagel I, Siebert R, Roschke AV, Sanger W, Wright GW, et al. Aberrant immunoglobulin class switch recombination and switch translocations in activated B cell-like diffuse large B cell lymphoma. J Exp Med 2007;204:633–43.
38. Bonetti P, Testoni M, Scandurra M, Ponzoni M, Piva R, Mensah AA, et al. Deregulation of ETS1 and FLI1 contributes to the pathogenesis of diffuse large B-cell lymphoma. Blood 2013;122:2233–41.
39. Zhang XK, Moussa O, LaRue A, Bradshaw S, Molano I, Spyropoulos DD, et al. The transcription factor Fli-1 modulates marginal zone and follicular B cell development in mice. J Immunol 2008;181:1644–54.
40. Xue HH, Bollenbacher-Reilley J, Wu Z, Spolski R, Jing X, Zhang YC, et al. The transcription factor GABP is a critical regulator of B lymphocyte development. Immunity 2007;26:421–31.
41. DeKoter RP, Geadah M, Khoosal S, Xu LS, Thillainadesan G, Torchia J, et al. Regulation of follicular B cell differentiation by the related E26 transformation-specific transcription factors PU.1, Spi-B, and Spi-C. J Immunol 2010;185:7374–84.
42. John SA, Clements JL, Russell LM, Garrett-Sinha LA. Ets-1 regulates plasma cell differentiation by interfering with the activity of the transcription factor Blimp-1. J Biol Chem 2008;283:951–62.
43. Lu D, Nakagawa R, Lazzaro S, Staudacher P, Abreu-Goodger C, Henley T, et al. The miR-155-PU.1 axis acts on Pax5 to enable efficient terminal B cell differentiation. J Exp Med 2014;211:2183–98.

44. Owen RG, Treon SP, Al-Katib A, Fonseca R, Greipp PR, McMaster ML, et al. Clinicopathological definition of Waldenstrom's macroglobulinemia: consensus panel recommendations from the Second International Workshop on Waldenstrom's Macroglobulinemia. Semin Oncol 2003;30:110–5.
45. Nguyen-Khac F, Lambert J, Chapiro E, Grelier A, Mould S, Barin C, et al. Chromosomal aberrations and their prognostic value in a series of 174 untreated patients with Waldenstrom's macroglobulinemia. Haematologica 2013;98:649–54.
46. Quek L, Otto GW, Garnett C, Lhermitte L, Karamitros D, Stoilova B, et al. Genetically distinct leukemic stem cells in human CD34- acute myeloid leukemia are arrested at a hemopoietic precursor-like stage. J Exp Med 2016;213:1513–35.
47. Malinge S, Ragu C, Della-Valle V, Pisani D, Constantinescu SN, Perez C, et al. Activating mutations in human acute megakaryoblastic leukemia. Blood 2008;112:4220–6.
48. Quivoron C, Couronne L, Della Valle V, Lopez CK, Plo I, Wagner-Ballon O, et al. TET2 inactivation results in pleiotropic hematopoietic abnormalities in mouse and is a recurrent event during human lymphomagenesis. Cancer Cell 2011;20:25–38.
49. Hallier M, Tavitian A, Moreau-Gachelin F. The transcription factor Spi-1/PU.1 binds RNA and interferes with the RNA-binding protein p54nrb. J Biol Chem 1996;271:11177–81.
50. Ridinger-Saison M, Boeva V, Rimmele P, Kulakovskiy I, Gallais I, Levavasseur B, et al. Spi-1/PU.1 activates transcription through clustered DNA occupancy in erythroleukemia. Nucleic Acids Res 2012;40:8927–41.